Downloaded from jnm.snmjournals.org by on March 15, 2017. For personal use only.

^{64}Cu-Labeled Folate-Conjugated Shell Cross-Linked Nanoparticles for Tumor Imaging and Radiotherapy: Synthesis, Radiolabeling, and Biologic Evaluation

Raffaella Rossin, PhD[1]; Dipanjan Pan, PhD[2]; Kai Qi, MS[2]; Jeffrey L. Turner, MA[2]; Xiankai Sun, PhD[1,3]; Karen L. Wooley, PhD[2]; and Michael J. Welch, PhD[1,2]

[1]Mallinckrodt Institute of Radiology, Washington University School of Medicine, St. Louis, Missouri; [2]Department of Chemistry, Washington University, St. Louis, Missouri; and [3]Department of Radiology, University of Texas Southwestern Medical Center, Dallas, Texas

Long-circulating nanoparticles functionalized with ligands for receptors overexpressed by tumor cells have promising applications for active and passive tumor targeting. The purpose of this study was to evaluate ^{64}Cu-radiolabeled folate-conjugated shell cross-linked nanoparticles (SCKs) as candidate agents to shuttle radionuclides and drugs into tumors overexpressing the folate receptor (FR). **Methods:** SCKs were obtained by cross-linking the shell of micelles obtained from amphiphilic diblock copolymers. SCKs were then functionalized with folate, fluorescein thiosemicarbazide (FTSC), and 1,4,8,11-tetraazacyclotetradecane-*N,N′,N″,N‴*-tetraacetic acid (TETA). The specific interaction of SCK-folate with the FR was investigated on KB cells. The biodistributions of ^{64}Cu-TETA-SCK and ^{64}Cu-TETA-SCK-folate were evaluated in athymic mice bearing small-size KB cell xenografts (10–100 mg), whereas the intratumor distributions were investigated by autoradiography in 0.3- to 0.6-g KB cell xenografts. **Results:** A global solution-state functionalization strategy has been introduced for attaching optimum numbers of targeting and imaging agents onto the SCKs for increasing the efficiency of interaction with cell-surface receptors. Epifluorescence microscopy confirmed the specific interaction of FTSC-SCK-folate with the FR in vitro. ^{64}Cu labeling of TETA-SCKs led to the radiolabeled compounds with 15%–20% yield and >95% radiochemical purity. The biodistribution results demonstrated high accumulation of ^{64}Cu-labeled SCKs in organs of the reticuloendothelial system (RES) (56.0 ± 7.1 %ID/g and 45.7 ± 3.5 %ID/g [percentage injected dose per gram] in liver at 10 min after injection for folated and nonfolated SCKs, respectively) and a prolonged blood circulation. No increase of SCK tumor uptake deriving from folate conjugation was observed (5.9 ± 2.8 %ID/g and 6.0 ± 1.9 %ID/g at 4 h after injection for folated and nonfolated SCKs, respectively). However, tumor accumulation was higher in small-size tumors, where competitive block of SCK-folate uptake with excess folate was observed. Autoradiography results confirmed the extravasation of radiolabeled SCKs in vascularized areas of the tumor, whereas no diffusion was observed in necrotic regions. **Conclusion:** Despite high RES uptake, the evaluated ^{64}Cu-labeled SCKs exhibited long circulation in blood and were able to passively accumulate in tumors. Furthermore, SCK-folate uptake was competitively blocked by excess folate in small-size solid tumors, suggesting interaction with the FR. For these reasons, functionalized SCKs are promising drug-delivery agents for imaging and therapy of early-stage solid tumors.

Key Words: ^{64}Cu; folate-nanoparticles; radiolabeling; folate receptor; enhanced permeability and retention effect

J Nucl Med 2005; 46:1210–1218

The development of intravenously administered nanoparticles for drug delivery and imaging of tumors and other malignancies has been a major challenge (*1*). Long-circulating nanoparticles are ideal vehicles for targeted drug delivery as their surface can be functionalized with a variety of ligands and proteins in a multivalent configuration, increasing the capability of interaction with the target. Furthermore, functional groups on the nanoparticle surface may be conjugated with metal-chelating systems for radiolabeling, thus providing effective tools for imaging and radiotherapy. Finally, the nanoparticle composition may be optimized to effectively encapsulate and release drugs, thus allowing both imaging and therapy with one vehicle (*2*).

Administered submicron particles are usually taken up by the macrophages of the reticuloendothelial system (RES), ending up in the liver, spleen, and lungs. However, a small size (<100 nm) and a hydrophilic surface can decrease nanoparticle opsonization and, consequently, slow down macrophages recognition (*1,3,4*).

To date, long-circulating nanoparticles have been evaluated mostly for delivery of antineoplastic agents such as doxorubicin, paclitaxel, 5-fluorouracil, irinotecan, and so forth, to solid tumors (*4,5*). Passively targeted delivery of

Received Jan. 13, 2005; revision accepted Mar. 29, 2005.

For correspondence or reprints contact: Michael J. Welch, PhD, Mallinckrodt Institute of Radiology, Washington University School of Medicine, 510 S. Kingshighway Blvd., Campus Box 8225, St. Louis, MO 63110.

E-mail: welchm@mir.wustl.edu

Downloaded from jnm.snmjournals.org by on March 15, 2017. For personal use only.

drugs takes advantage of a defective vascular architecture caused by rapid tumor vascularization (angiogenesis), which is necessary for nutrient and oxygen supply and for waste disposal in fast-growing tumors (*6*). Blood vessels in solid tumors are highly permeable because of unusually large gaps (~300–800 nm) between adjacent endothelial cells caused by an abnormal arrangement of basement membrane and perivascular cells (*7*). However, a chaotic and disorganized branched vessel system and a high interstitial pressure result in pockets of nonaccessible cancer cells and make extravasation of blood-borne drugs difficult (*6*). Nonetheless, since tumors exhibit an impaired lymphatic system (*8*), macromolecules escaping RES sequestration may leak out of the permeable blood vessels and accumulate for a long time in perivascular tumor tissues (enhanced permeability and retention [EPR] effect) (*4,5*).

Alternative targeting approaches exploit the existence on target cells of molecular signatures for various pathologies. Thus, conjugation of ligands with high affinity for receptors, antigens, and so forth, overexpressed by tumor cells may allow early assessment and therapy of pathologies on a molecular level while decreasing cytotoxicity to normal tissues. To date, a variety of nanoparticles (nanospheres, nanocapsules, liposomes, dendrimers, and so forth) have been functionalized mainly with ligands and antibodies targeting endothelial receptors on tumor-proliferating microvasculature (*2,9–13*), the prostate-specific membrane antigen on prostate cancer cells (*14,15*), and the folate receptor (FR) (*16–22*).

The FR, or membrane-associated folate-binding protein, is 1 of the 2 existing cellular folate transport systems and binds physiologic folates with affinity in the nanomolar range (*23*). FR is an attractive molecular target for tumor targeting because it is overexpressed by several tumor cells (e.g., ovarian, colorectal, breast, nasopharyngeal carcinomas, and so forth), though it has only limited expression in most normal tissues (*23,24*). The feasibility of FR-mediated tumor delivery of drugs for therapy (*22,25*), of radionuclides for imaging (*26*), of vectors for gene delivery (*21*), and so forth, has been recently reviewed.

In this study, we evaluated in vivo and in vitro a new folate-conjugated polymeric nanoparticle for tumor targeting via both FR-mediated endocytosis and the EPR effect. Shell cross-linked nanoparticles (SCKs) are core-shell nanospheres inspired from biologic constructs and optimized for guest packaging (*27*). Stable SCKs are obtained by cross-linking the shell layer of micelles derived from the self-assembly of amphiphilic diblock copolymers in aqueous solution. Control over the synthesis of the diblock copolymers and the micellar formation conditions affords SCKs with well-defined size, surface charge, hydrophilicity, shape adaptability, and available functionality (*27*). To date, the SCK surface has been straightforwardly decorated with a variety of receptor ligands (*13,17,28*).

To evaluate the in vivo behavior of folate-SCKs, we have chosen ^{64}Cu radiolabeling. ^{64}Cu (half-life [$t_{1/2}$] = 12.7 h) has been extensively studied for the production of radiopharmaceuticals for both PET and radiotherapy in the past 2 decades because of its radioactive decay with β^+ (17%) and β^- (40%) emission (*29*). At Washington University School of Medicine, no-carrier-added ^{64}Cu is produced on a biomedical cyclotron with a high specific activity, suitable for receptor-targeting studies (*30*). For ^{64}Cu-labeling purposes, the SCK-folate surface has been functionalized with 1,4,8,11-tetraazacyclotetradecane-*N,N′,N″,N‴*-tetraacetic acid (TETA), a macrocyclic ligand that provides the copper complex kinetic and thermodynamic stabilty in vivo (*29*). Then, we evaluated the ^{64}Cu-labeled SCK-folate nanoparticles in vivo in a tumor model overexpressing the FR (*31*). Biodistribution and autoradiography studies were performed to compare uptake and distribution of FR-targeted and nontargeted SCKs in KB tumor cell xenografts, thus evaluating the contribution of the EPR effect and FR-interaction to the tumor targeting. The present study is expected to have relevance in the understanding of active versus passive targeting of solid tumors via engineered nanoparticles. Furthermore, ^{64}Cu-labeled nanoparticles may have the potential to deliver high concentration of radionuclide to solid tumors together with cytotoxic drugs, thereby enhancing the therapeutic efficacy and allowing imaging at the same time.

MATERIALS AND METHODS

Reagents

Unless otherwise listed, all solvents and reagents were purchased from Sigma-Aldrich and used as received. Methanol, sodium hydroxide, and hydrochloric acid solutions were purchased from Fisher Scientific. Tween 20 solution (10%) was purchased from Bio-Rad. Spectra/Por membrane (12- to 14-kDa molecular weight cutoff) used for dialysis was obtained from Spectrum Medical Industries, Inc. Water was distilled and then deionized (18 MΩ/cm^2) by passing through a Milli-Q water filtration system (Millipore Corp.). The buffer solution used for ^{64}Cu-labeling reactions (0.1 mol/L ammonium acetate, pH 5.5) was further purified on Chelex 100 resin (Bio-Rad) before use. Centricon YM-100 tubes (100-kDa molecular weight cutoff) were purchased from Millipore Corp.

^{64}Cu was prepared on the Washington University Medical School CS-15 cyclotron by the ^{64}Ni(p,n)^{64}Cu nuclear reaction at a specific activity of 47.4–474 GBq/μmol at the end of bombardment as previously described (*30*).

Synthesis of SCK and SCK-Folate

SCKs were prepared following a previously reported procedure (*32*). Briefly, the micelles were prepared in 2 steps from the diblock copolymer poly(acrylic acid-b-methyl acrylate) (PAA_{93}-b-PMA_{164}), as illustrated in Figure 1, followed by intramicellar crosslinking (20%) to produce shell cross-linked nanoparticles. A folate-$PEG_{1,600}$-amine ($PEG_{1,600}$ is a poly(ethylene glycol) spacer with a molecular weight of 1,600 Da) was also synthesized from folic acid and conjugated onto the shell surface of the SCKs by activating a portion of the available carboxylic acids with 1-(3′-dimethylaminopropyl)-3-ethylcarbodiimide (EDC) methiodide (*13,17*).

Downloaded from jnm.snmjournals.org by on March 15, 2017. For personal use only.

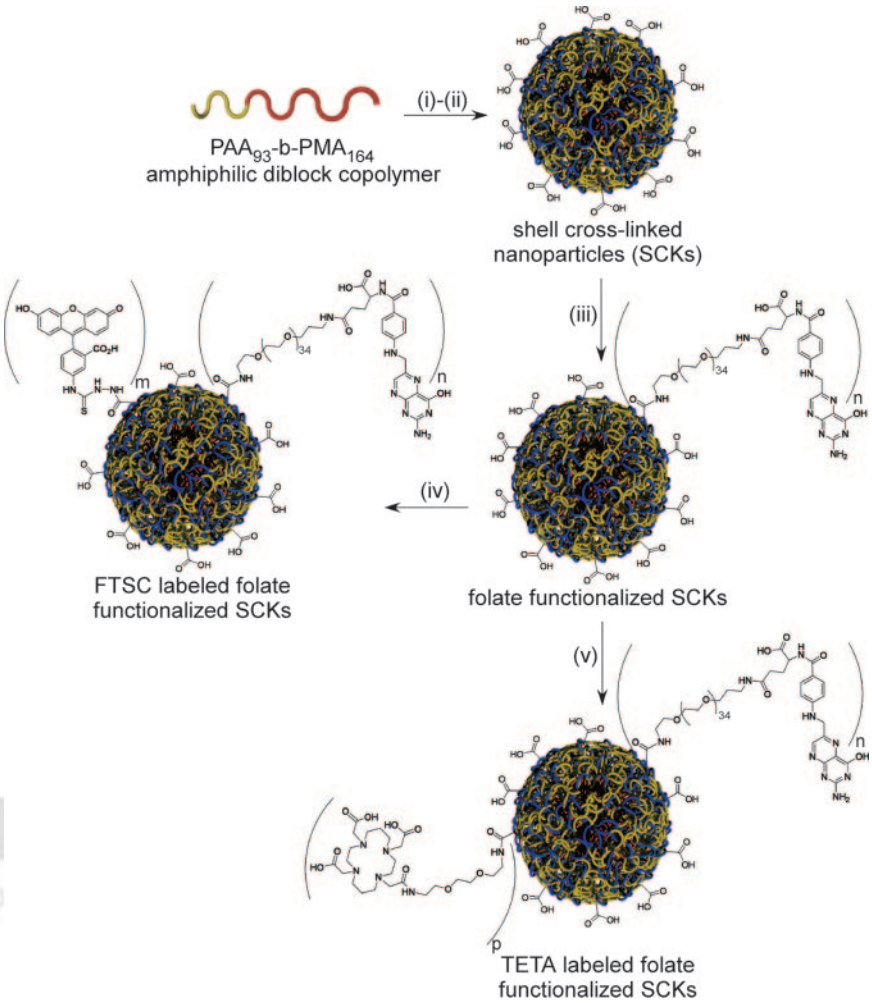

FIGURE 1. Preparation of SCKs functionalized with folate for targeting and labeled with FTSC or TETA for fluorescence or radionuclide detection, respectively. Reagents and conditions: (i) polymer micelle formation: tetrahydrofuran, followed by controlled addition of water and dialysis against water; (ii) shell crosslinking: block copolymer micelles, 2,2′-(ethylenedioxy)-bis(ethylamine), 1-(3′-dimethylaminopropyl)-3-ethylcarbodiimide (EDC) methiodide, room temperature (RT), followed by dialysis against water; (iii) shell functionalization with folate-$PEG_{1,600}$-amine ($PEG_{1,600}$ is a poly(ethylene glycol) spacer with a molecular weight of 1,600 Da): nonfunctionalized SCKs, folate-$PEG_{1,600}$-amine, EDC methiodide, RT, followed by dialysis against sodium phosphate-buffered saline at pH 7.3; (iv) shell functionalization with fluorescein thiosemicarbazide (FTSC): SCK-folate, FTSC, EDC methiodide, RT, followed by dialysis against sodium phosphate-buffered saline at pH 7.3; (v) shell functionalization with TETA-amine: SCK-folate, sulfo-NHS (s-NHS), EDC, 4°C, 2 h, followed by Centricon separation, TETA-amine, 4°C, overnight.

Synthesis of FTSC-Conjugated SCK and SCK-Folate

SCKs and folate-$PEG_{1,600}$ derivatized SCKs were further functionalized with fluorescein thiosemicarbazide (FTSC) following a reported procedure (*13,28*) to afford folate-targeted and FTSC-labeled nanoparticles.

Synthesis of TETA-NH_2

TETA-NH_2 was synthesized in a straightforward way from TETA. Briefly, a mono *tert*-Boc–protected diamine (*N*-butoxycarbonyl-[2,2′-(ethylenedioxy)bis(ethylamine)]) was allowed to react with TETA in the presence of EDC for a period of 16 h. The protected intermediate was then isolated, the *tert*-Boc protecting group was cleaved with trifluoroacetic acid, and the TETA-NH_2 product was then purified by repeated precipitation from methanol and acetone.

TETA Functionalization of SCK and SCK-Folate

The conjugation was done by a modified procedure developed for 1,4,7,10-tetraazacyclododecane-*N,N′,N″,N‴*-tetraacetic acid (DOTA)-protein conjugation via the *N*-hydroxysuccinimide route (*33*). Briefly, the carboxylic groups on the SCK and SCK-folate shells were activated by adding EDC (2 equivalents with respect to the carboxylate groups) and *N*-hydroxysulfosuccinimide sodium salt (s-NHS) (4 equivalents with respect to the carboxylate groups). The activation reactions were performed in 10 mmol/L phosphate-buffered saline (PBS) solution (pH adjusted to 5.5) at 4°C for 2 h under gentle stirring. The s-NHS-SCKs were separated from excess EDC and s-NHS by Centricon YM-100 and the residues were extensively washed with PBS solution. The activated esters were reconstituted in 10 mmol/L PBS (pH 7.4) and then functionalized with TETA-NH_2 (4 equivalents with respect to the carboxylate groups). The solution pH was adjusted to 8, and then the reaction mixtures were gently stirred at 4°C overnight. After TETA conjugation, the nanoparticle solutions were again concentrated by Centricon YM-100 and the residues were extensively washed with PBS to ensure complete separation from the unreacted TETA-NH_2. Finally, the residues were reconstituted to 0.2–0.3 mg/mL solutions in 10 mmol/L PBS, pH 7.4, and stored at 4°C for further use.

Radiolabeling of TETA-SCK Conjugates with ^{64}Cu

^{64}Cu chloride (typically in 0.1 mol/L HCl) was converted to ^{64}Cu acetate by adding 100 μL of 0.1 mol/L ammonium acetate buffer, pH 6.5. To 500 μL of the TETA-SCK solutions (in 10 mmol/L PBS, pH 7.4, containing 0.05% Tween 20), 50 μL of ^{64}Cu acetate was added (~185 MBq). The resulting solutions were incubated at 43°C for 2.5 h in a thermomixer (1,000 rpm). After incubation, the ^{64}Cu/TETA-SCK solutions were added with 5 μL of 10 mmol/L diethylenetriaminepentaacetic acid (DTPA) and incubated for 10 min at room temperature. Radiochemical purity (RCP) of the ^{64}Cu-labeled SCKs was determined by thin-layer

Downloaded from jnm.snmjournals.org by on March 15, 2017. For personal use only.

chromatography (TLC) analysis after DTPA challenge, Centricon concentration, and washing. The solutions were spotted on silica gel TLC plates (Fisher Scientific), which were developed in methanol/10% ammonium acetate (v/v, 1:1) and analyzed by a Bioscan 200 imaging scanner (Bioscan Inc.). The ^{64}Cu-labeled SCK remained at the origin, whereas the residual ^{64}Cu-DTPA complex migrated with an R_f of 0.5 (labeling yield, 15%–20%, decay corrected; RCP, >95%). The products were then diluted with 0.05% Tween 20 solution in 10 mmol/L PBS, pH 7.4, to prepare appropriate doses for biodistribution and autoradiography studies.

Cell Culture

KB cells, a human nasopharyngeal epidermal carcinoma cell line overexpressing the FR (*34*), were obtained from American Type Culture Collection and cultured continuously as a monolayer at 37°C in a humified atmosphere containing 5% CO_2 in folate-deficient modified Eagle's medium (FDMEM) (a folate-free modified Eagle's medium supplemented with 10% [v/v] heat-inactivated fetal bovine serum as only source of folate) containing 2 mmol/L L-glutamine.

Athymic Mouse Tumor Model

All animal studies were performed in compliance with guidelines set by the Washington University Animal Studies Committee. Three- to 4-wk-old female athymic *nu/nu* mice (Charles Rivers Laboratories) were used. After 1 or 2 wk on a folate-deficient rodent chow diet (ICN Biochemicals), mice were inoculated subcutaneously with 0.1 mL of KB cell suspension (1×10^6 cells per mouse) into the nape of the neck. SCK biodistribution studies were performed 1 wk after tumor cell implantation, when tumors reached ~10- to 100-mg weight. For autoradiography studies, tumors were allowed to grow for 2 wk until they reached a 0.3- to 0.6-g weight. In both cases, mice were on a folate-deficient diet for 3 wk before radiotracer administration. Experiments with competitive block of the FR were performed by feeding the mice a normal rodent chow for 24 h and by administering them free folic acid (1 mg/100 μL 0.2 mol/L $NaHCO_3$, by intraperitoneal injection) 24 h and 1 h before radiotracer administration.

In Vitro Cell Studies

KB cells in FDMEM were transferred to 33-mm culture dishes at 3×10^5 cells per dish 24 h before the assay. The cells were then rinsed with PBS (1 mL) and incubated for 4 h at 37°C or 4°C with 10 μg/mL of FTSC-SCK-folate diluted in culture medium. In free folate competition studies, 1 mmol/L folic acid was added to the incubation medium. After washing with PBS (3 × 1 mL) to remove free nanoparticles, cell-associated fluorescence was imaged by epifluorescence microscopy (Olympus IX-70 inverted microscope; Hitschfel Instruments Inc.). An argon laser for FTSC excitation at 488 nm was used for imaging.

Biodistribution Studies

^{64}Cu-Labeled SCK and SCK-folate were diluted with 0.05% Tween 20 solution in 10 mmol/L PBS, pH 7.4. The KB tumor cell xenograft-bearing mice weighing 20–25 g ($n = 4$ per time point) were anesthetized with isoflurane and injected intravenously with 370–440 kBq of labeled nanoparticles (3–5 mg/kg mouse weight) in 100 μL via the tail vein. The mice were anesthetized before sacrifice (by cervical dislocation) at each time point. Organs of interest were removed and weighed, and sample radioactivity was measured. Standards were prepared and measured along with the samples to calculate the percentage injected dose per gram of tissue (%ID/g) and the percentage injected dose per organ (%ID/organ).

Autoradiography Studies

A 100-μL solution containing 1.85 MBq ^{64}Cu-labeled SCK or SCK-folate (~5 mg/kg mouse weight) was administered intravenously to KB tumor cell xenograft- bearing mice anesthetized with isoflurane ($n = 2$). The mice were then allowed access to food and water ad libitum. At 23 h after injection, the mice were anesthetized again and administered ^{18}F-FDG (18.5 MBq in 100 μL) intravenously. At 24 h after injection, the mice were anesthetized and sacrificed by cervical dislocation. KB tumors were resected and sliced into 1-mm sections. Digital autoradiographs defining the intratumoral distribution of ^{18}F radiotracer were collected (Canberra Packard Instant Imager; Canberra Industries Inc.) in a 2-min acquisition period shortly after the tumor was sectioned. After a 20-h delay, ^{64}Cu images were collected with a 6-h acquisition period.

RESULTS

Synthesis and Functionalization of SCKs

Micelles were assembled from amphiphilic block copolymer PAA_{93}-b-PMA_{164}, which was prepared by sequential atom transfer radical polymerization of *tert*-butyl acrylate and methyl acrylate, followed by acidolysis of the *tert*-butyl esters (Fig. 1). Shell cross-linking of the micelle was achieved by intramicellar conversion (20%) of available acrylic acid residues in the shell layer to amides, which was accomplished by the carbodiimide-mediated reaction with a diamino crosslinker. A previously prepared folate-$PEG_{1,600}$-amine was then used for the conjugation of the folic acid group onto the SCKs (*17*). A $PEG_{1,600}$ spacer was used to provide for the folate groups to be bioavailable for interaction with the FR. A fraction (1%) of the available COOH groups of SCKs was activated with 1-(3′-dimethylaminopropyl)-3-ethylcarbodiimide methiodide and then allowed to undergo reaction with folate-$PEG_{1,600}$-amine. This resulted in nominally 90 folates per SCK nanoparticle. Detailed characterization of the nanoparticles was performed by multiple analytic techniques, such as dynamic light scattering (DLS), transmission electron microscopy, electrophoretic light scattering (ZETA potential measurements), ultraviolet-visible spectroscopy, fluorescence spectroscopy, and so forth.

In Vitro Binding Studies

SCK-folate nanoparticles were labeled with FTSC and cell uptake was evaluated by epifluorescence microscopy after incubation of KB cells with 10 μg of nanoparticles at 37°C and 4°C. After 4 h of incubation at 37°C, folate-conjugated SCKs were found to bind KB cells and the fluorescence images suggest the presence of FTSC-SCK-folate–containing vesicles within the cytoplasm (Fig. 2A). After 4 h of incubation at 4°C, uptake of folate-conjugated SCKs on the KB cell surface was clearly visible, but no fluorescent vesicles were observed inside the cell (Fig. 2C). In both cases, FTSC-SCK-folate uptake could be blocked if

Downloaded from jnm.snmjournals.org by on March 15, 2017. For personal use only.

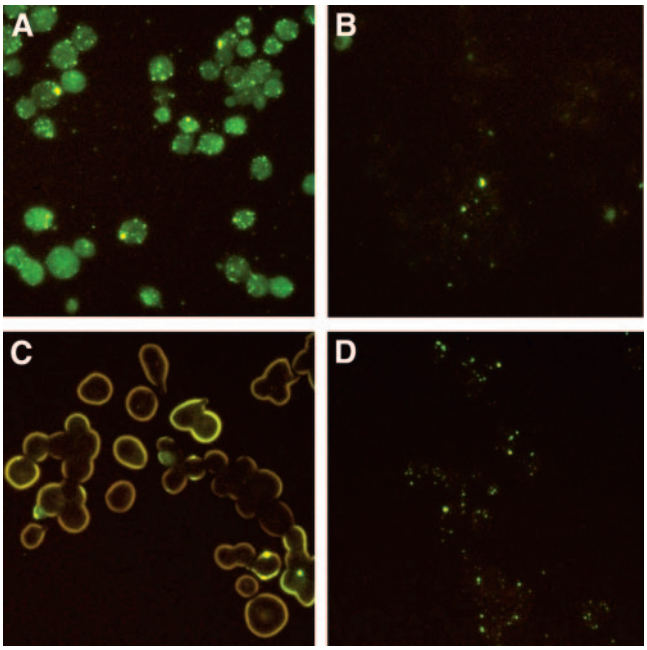

FIGURE 2. Fluorescence micrographs of KB cells incubated for 4 h at 37°C (A and B) and 4°C (C and D) with FTSC and folate-conjugated SCKs (10 μg FTSC-SCK-folate per 33-mm culture dish, plated with 3×10^5 cells per dish 24 h before assay). Incubation at 4°C led to surface uptake of FTSC-SCK-folate onto KB cells (C), whereas fluorescent endocytotic vesicles are visible inside the cells after 4 h of incubation at 37°C (A). At both incubation temperatures, excess folic acid (1 mmol/L) competitively inhibited FTSC-SCK-folate cell uptake (B and D).

free folate (1 mmol/L) was added to the binding medium during incubation (Figs. 2B and 2D).

Radiolabeling of SCKs with ^{64}Cu

TETA-SCK and TETA-SCK-folate were effectively radiolabeled with ^{64}Cu acetate under mild reaction conditions (2.5 h at 43°C, pH 7.4). DTPA was added to the labeling mixture to remove the nonspecifically bound ^{64}Cu from the SCK surface. Centricon concentration followed by 2 rinsing cycles (with 0.05% Tween 20 in 10 mmol/L PBS) afforded both ^{64}Cu-labeled nanoconjugates with a high RCP (>95%), as confirmed by radio-TLC analysis. The final labeling yield was 15%–20%, decay corrected.

Biodistribution Studies

Tables 1 and 2 present a summary of the biodistribution data for the ^{64}Cu-TETA-SCK-folate and ^{64}Cu-TETA-SCK conjugates in athymic *nu/nu* mice bearing small KB tumor cell xenografts (~10–100 mg). Twenty mice were administered each radiolabeled nanoparticle. After intravenous injection, blood clearance was rapid and, after 10 min, blood uptake was constant (~2–3 %ID/g) over the considered time points. For both nanoparticles, the highest %ID went to organs of the RES. Both SCKs were taken up rapidly by the liver (56.0 ± 7.1 %ID/g and 45.7 ± 3.5 %ID/g at 10 min after injection for SCK-folate and SCK, respectively) and were then slowly cleared through the intestine (21.5 ± 2.9 %ID/g and 26.9 ± 3.9 %ID/g liver uptake at 24 h after injection for SCK-folate and SCK, respectively). Similarly, spleen uptake was high shortly after nanoparticle administration (18.3 ± 6.3 %ID/g and 11.5 ± 2.5 %ID/g at 10 min after injection for SCK-folate and SCK, respectively) and then slowly decreased over time (4.7 ± 1.0 %ID/g and 4.5 ± 0.6 %ID/g at 24 h after injection for SCK-folate and SCK, respectively). ^{64}Cu-Labeled SCKs were found to accumulate in lungs at 10 min after injection (39.7 ± 5.1 %ID/g and 32.5 ± 14.0 %ID/g for SCK-folate and SCK, respectively). However, unlike the liver and spleen, lung uptake of the SCK-folate was found to rapidly decrease within 1 h after injection (10.9 ± 3.8 %ID/g; $P = 0.0001$) and then remained constant throughout the rest of the experiment. Lung uptake of the SCK alone showed a similar profile, with a slightly slower clearance compared with the folate conjugate (15.0 ± 4.1 %ID/g and 12.7 ± 1.8 %ID/g at 1 and 24 h after injection, respectively). Among the non-RES organs, kidneys showed the same level of SCK-folate uptake over time (~8–10 %ID/g), whereas heart uptake slightly increased from 2.3 ± 0.2 %ID/g at 10 min after injection to 4.3 ± 0.5 %ID/g at 24 h after injection. SCK uptake in these organs was slightly higher, yet with similar time distribution profiles.

TABLE 1
Biodistribution Data of ^{64}Cu-TETA-SCK-Folate in KB Tumor Cell Xenograft-Bearing Athymic Nude Female Mice ($n = 4$)

	%ID/g				%ID/organ			
Biodistribution	10 min	1 h	4 h	24 h	10 min	1 h	4 h	24 h
Blood	2.1 ± 0.2	2.1 ± 0.2	2.5 ± 0.3	2.6 ± 0.6	3.1 ± 0.2	3.4 ± 0.2	4.2 ± 0.3	4.3 ± 0.9
Lung	39.7 ± 5.1	10.9 ± 3.8	14.4 ± 5.9	10.8 ± 1.4	5.1 ± 0.9	1.5 ± 0.2	2.1 ± 0.9	1.5 ± 0.2
Liver	56.0 ± 7.1	38.4 ± 7.9	33.8 ± 2.6	21.5 ± 2.9	52.3 ± 5.6	41.7 ± 3.0	34.1 ± 2.5	25.2 ± 2.9
Spleen	18.3 ± 6.3	10.8 ± 3.2	8.8 ± 0.5	4.7 ± 1.0	1.5 ± 0.4	1.0 ± 0.3	0.8 ± 0.2	0.5 ± 0.2
Kidney	7.2 ± 1.6	8.1 ± 1.8	7.9 ± 0.8	8.5 ± 1.3	1.2 ± 0.3	1.3 ± 0.2	1.4 ± 0.2	1.5 ± 0.4
Muscle	0.8 ± 0.1	0.8 ± 0.2	0.9 ± 0.2	1.0 ± 0.1	7.2 ± 0.5	7.5 ± 1.3	8.6 ± 1.7	9.5 ± 1.3
Heart	2.3 ± 0.2	2.7 ± 0.5	3.7 ± 0.3	4.3 ± 0.5	0.2 ± 0.0	0.3 ± 0.1	0.4 ± 0.0	0.5 ± 0.0
Tumor	3.4 ± 1.2	2.3 ± 0.7	5.9 ± 2.8	2.9 ± 3.1	0.04 ± 0.02	0.12 ± 0.02	0.04 ± 0.02	0.09 ± 0.07

Data are presented as percentage injected dose per gram (%ID/g) and percentage injected dose per organ (%ID/organ) ± SD.

Downloaded from jnm.snmjournals.org by on March 15, 2017. For personal use only.

TABLE 2
Biodistribution Data of ^{64}Cu-TETA-SCK in KB Tumor Cell Xenograft-Bearing Athymic Nude Female Mice (n = 4)

	%ID/g				%ID/organ			
Biodistribution	10 min	1 h	4 h	24 h	10 min	1 h	4 h	24 h
Blood	3.3 ± 0.3	2.4 ± 0.7	2.6 ± 0.8	3.1 ± 0.3	5.1 ± 0.4	3.7 ± 0.8	3.8 ± 1.3	4.8 ± 0.2
Lung	32.5 ± 14.0	15.0 ± 4.1	13.8 ± 6.6	12.7 ± 1.8	4.6 ± 1.8	1.9 ± 0.3	1.8 ± 0.9	1.8 ± 0.1
Liver	45.7 ± 3.5	35.3 ± 8.8	31.8 ± 11.9	26.9 ± 3.9	45.6 ± 2.5	34.3 ± 7.3	27.3 ± 10.2	26.1 ± 1.0
Spleen	11.5 ± 2.5	8.2 ± 3.4	4.7 ± 2.0	4.5 ± 0.6	1.0 ± 0.2	0.8 ± 0.3	0.4 ± 0.2	0.4 ± 0.1
Kidney	9.0 ± 0.6	8.6 ± 2.0	9.5 ± 0.8	10.8 ± 1.1	1.5 ± 0.0	1.4 ± 0.4	1.4 ± 0.3	1.7 ± 0.1
Muscle	1.1 ± 0.1	0.9 ± 0.2	0.9 ± 0.2	1.4 ± 0.2	10.1 ± 0.2	8.4 ± 2.0	7.6 ± 1.9	13.1 ± 2.6
Heart	3.7 ± 0.1	4.0 ± 1.3	4.7 ± 1.5	6.2 ± 0.4	0.4 ± 0.0	0.5 ± 0.2	0.4 ± 0.2	0.6 ± 0.0
Tumor	2.2 ± 0.3	3.2 ± 0.7	6.0 ± 1.9	5.6 ± 0.9	0.04 ± 0.04	0.17 ± 0.07	0.13 ± 0.04	0.18 ± 0.11

Data are presented as percentage injected dose per gram (%ID/g) and percentage injected dose per organ (%ID/organ) ± SD.

The tumor targeting obtained with ^{64}Cu-TETA-SCK-folate was highly variable within the groups of mice (Table 1), with variations not depending on sacrifice time after injection (3.4 ± 1.2 %ID/g, 2.3 ± 0.7 %ID/g, 5.9 ± 2.8 %ID/g, and 2.9 ± 3.1 %ID/g at 10 min, 1 h, 4 h, and 24 h after injection, respectively). However, by considering the tumor weights (1–50 mg) in the animal group sacrificed at 4 h after injection (Fig. 3A), great variability was observed in tumors with different size and an inverse correlation between specific tumor uptake and tumor weight was apparent. Furthermore, by comparing these results with tumor uptake in mice coadministered with excess folic acid, competitive block of SCK-folate tumor uptake in FR-overexpressing tumors was observed. The specific tumor uptake of radiolabeled SCK was dependent on tumor size as well, although it was less variable within each animal group compared with the folate conjugate (2.1 ± 0.3 %ID/g, 3.2 ± 0.7 %ID/g, 6.0 ± 1.9 %ID/g, and 5.6 ± 0.9 %ID/g at 10 min, 1 h, 4 h, and 24 h after injection, respectively). However, no competitive block of nanoparticle tumor uptake was observed after coadministration of ^{64}Cu-TETA-SCK and excess folic acid (Fig. 3B).

Autoradiography Studies

The mice used for digital autoradiography were implanted subcutaneously with KB cells (1 × 10^6 cells/100 μL) 2 wk before the experiment, so that 0.3- to 0.6-g weight tumors were obtained. Mice were administered intravenous ^{64}Cu-TETA-SCK-folate or ^{64}Cu-TETA-SCK (1.85 MBq, ~5 mg/kg mouse weight) 24 h before sacrifice, to allow nanoparticle accumulation at the tumor site. Tissue distribution of nanoparticles was compared with ^{18}F-FDG distribution by administering the mice with the ^{18}F-labeled radiotracer (18.5 MBq) 1 h before animal sacrifice and tumor resection. Homogeneity of ^{18}F-FDG and nanoparticle localization was evaluated on 1-mm tumor sections by acquiring images shortly after tumor resection and 20 h later, to allow for ^{18}F decay. The collected images, depicted in Figure 4, showed nonhomogeneous distribution of both ^{64}Cu-labeled nanoparticles and ^{18}F-FDG within the tumor, with areas exhibiting no accumulation of either radiotracer. Furthermore, distribution of radiolabeled SCK was not in complete accordance with ^{18}F-FDG distribution.

DISCUSSION

The studies reported herein focus on the evaluation of cell uptake, biodistribution, and tumor retention of polymeric nanoparticles as possible vehicles for drug delivery and tumor imaging via both the interaction with the FR and the EPR effect. Small-size SCKs were obtained by crosslinking the outer shell of micelles deriving from the self-assembly of amphiphilic diblock copolymers (Fig. 1), as described previously (*32*). The average SCK size (20 ± 3 nm, DLS)

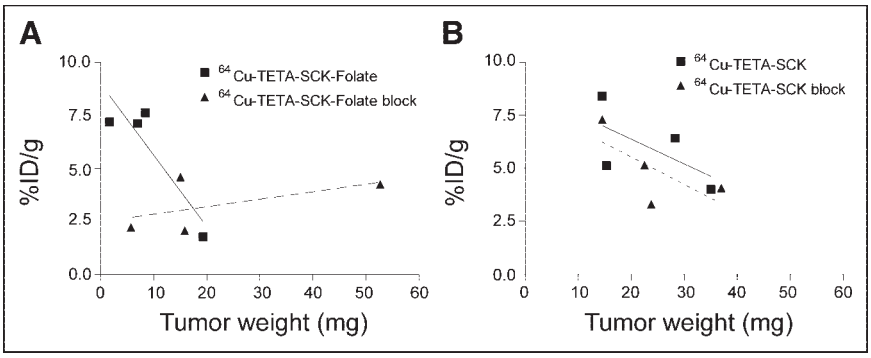

FIGURE 3. Dependence of tumor uptake on tumor size 4 h after injection of ^{64}Cu-labeled folated (A) and nonfolated (B) SCKs in KB xenograft-bearing mice. Data are presented as %ID/g. Within each experimental group, small tumors exhibited enhanced nanoparticle uptake. Coadministration of excess folic acid led to competitive block of ^{64}Cu-TETA-SCK-folate tumor uptake (A, dashed line), whereas it had no noticeable effect on ^{64}Cu-TETA-SCK tumor uptake (B, dashed line).

Downloaded from jnm.snmjournals.org by on March 15, 2017. For personal use only.

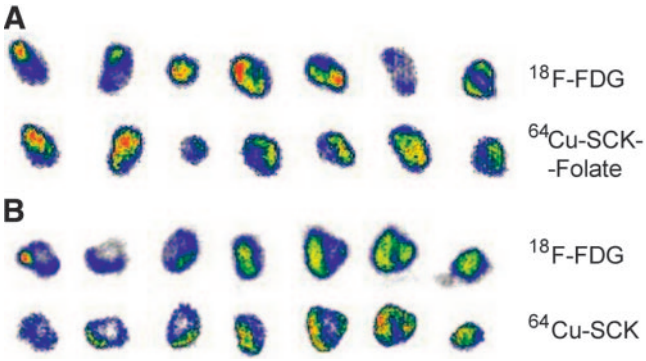

FIGURE 4. Dual-tracer autoradiographs demonstrate regional concentration of ^{64}Cu-labeled folated (A) or nonfolated (B) SCKs in mice bearing 0.3- to 0.6-g KB xenografts. Tumors were resected and sectioned into 1-mm slices 1 h after ^{18}F-FDG administration and 24 h after administration of ^{64}Cu-radiolabeled SCKs. Images of ^{18}F-FDG distribution were collected shortly after tumor resection, whereas distribution of ^{64}Cu-labeled SCKs in the same slices was imaged with a 20-h delay. Both tumors exhibit scattered necrotic regions (no radiotracer uptake).

and the hydrophilic surface (polyacrylic acid) were considered suitable for passive tumor targeting, based on published studies on long-circulating nanoparticles (*1,3,4*). Furthermore, we functionalized the SCK surface with folic acid to evaluate receptor-mediated tumor targeting with SCKs (*17*).

The FR is an attractive molecular target for radionuclide and drug delivery, since it is overexpressed by a panel of human cancers (*23,24*) and, in particular, by >90% of ovarian carcinomas, where receptor levels increase with tumor aggressiveness and grade (*26*).

A poly(ethylene glycol) (PEG) spacer with 34 repeat units (molecular weight, 1,600 Da) was introduced with the folic acid. Total numbers of ligands attached to the shell surface of these nanoparticles is another important parameter to achieve greater efficiency of interaction of nanoparticles with the cell-surface receptors. A theoretic calculation based on a procedure reported in the literature (*35*) showed that a total number of 20–70 folate-$PEG_{1,600}$ is required to completely cover the surface of these 20 ± 3 nm nanoparticles. As a consequence, we functionalized 1% of the available COOH groups on the SCK surface, thus obtaining a nominal number of 90 folate-$PEG_{1,600}$ per SCK, which is within the calculated range of the ligands to cover the whole surface.

Conjugation of FTSC on the nanoparticle surface allowed direct visualization of SCK-folate uptake in tumor cells in vitro by means of epifluorescence microscopy. The fluorescence images in Figure 2 show KB cells after 4 h of incubation in a solution containing FTSC-SCK-folate at 37°C (Fig. 2A) and at 4°C (Fig. 2C). In both cases, SCK-folate uptake on the cell surface is clearly visible. However, after incubation at 37°C, brightly fluorescent spots were visible inside the cells, suggesting the presence of SCK-folate in endocytotic vesicles. In contrast, after incubation at 4°C (temperature at which internalization is inhibited), no intracellular vesicles were visible and fluorescence was mainly limited to the cell surface. Furthermore, SCK-folate uptake at both 37°C and 4°C could be blocked if free folate (1 mmol/L) was added to the FTSC-SCK-folate solution during incubation (Figs. 2B and 2D). These findings confirm FR-mediated interaction between SCK-folate and FR-overexpressing tumor cells and suggest FR-mediated endocytosis in vitro, as previously observed for folate-conjugated liposomes (*22*) and other nanoparticles (*20*).

^{64}Cu radiolabeling of SCK and SCK-folate was straightforward after TETA-NH_2 conjugation. However, significant adsorption of ^{64}Cu on the SCK surface was observed and a DTPA challenge was necessary to remove nonspecifically bound ^{64}Cu activity from the nanoconjugates. As a consequence, moderate radiolabeling yields were achieved (15%–20%, decay corrected), but the high RCP (>95%, after DTPA challenge and Centricon purification) and the chemical stability (>60% intact ^{64}Cu-TETA-SCK after 24 h of incubation at 37°C in PBS, as confirmed by radio-TLC analysis) were considered suitable for in vivo studies.

SCK-folate biodistribution and tumor-targeting capability were investigated in athymic *nu/nu* female mice bearing KB tumor cell xenografts. We chose 1-wk-old, small-size KB xenografts (~10–100 mg) grown subcutaneously in the nape of the neck in mice to evaluate the possible use of nanoparticles to target early-stage solid tumors in vivo. Mice were kept on a folate-depleted diet before (3 wk) and during the experiments to achieve plasma folate levels in the physiologic range normally seen for humans (*18*). One day and again 1 h before each experiment, a group of mice was administered intraperitoneally excess folic acid to raise the plasma folate level and to evaluate the effects of competitive block of the FR on the SCK tumor uptake. As shown in Tables 1 and 2, administration of both folated and nonfolated ^{64}Cu-labeled SCKs led to a rapid and extensive RES uptake. Folated SCKs showed higher accumulation in liver compared with nonfolated SCKs, reasonably because of higher opsonization and macrophage recognition after folate conjugation or to direct recognition by the liver FR (Kupffer cell receptor–mediated endocytosis). Both SCK-folate and SCK exhibited also immediate lung uptake, probably due to sequestration of some aggregated nanoparticles by the lung capillary bed after intravenous injection. However, clearance of radiolabeled nanoparticles from lungs was fast and lung uptake values at 1 h after injection were in the range previously observed with other SCKs (data not shown).

Notwithstanding high RES uptake, the biodistribution data showed that SCKs had prolonged blood retention properties. Both folated and nonfolated SCKs were present in the blood at 24 h after injection (2.6 ± 0.6 %ID/g and 3.1 ± 0.3 %ID/g, respectively), with a slightly lower blood level of ^{64}Cu-TETA-SCK-folate compared with the nonfolated conjugate due to higher liver uptake. As a result of the pro-

Downloaded from jnm.snmjournals.org by on March 15, 2017. For personal use only.

longed blood circulation, mice treated with radiolabeled SCKs showed in vivo tumor accumulation of radioactivity. However, the biodistribution data showed no evidence of the benefit of folate conjugation on in vivo accumulation of nanoparticles in FR-overexpressing tumors (Tables 1 and 2). Furthermore, the specific tumor uptake of both nanoparticles exhibited high variability within the groups of mice, resulting in high SDs.

Lack of selectivity of folate-conjugated nanoparticles and liposomes over nonfolated conjugates for FR-overexpressing solid tumors has been previously reported by other researchers (*18,19,22,36,37*). This is a result of passive extravasation from the permeable tumor blood vessels (EPR effect), which is the rate-determining step driving accumulation of long-circulating macromolecules in solid tumors. However, selective interaction of folated liposomes with FR-overexpressing cells in vivo has been demonstrated in ascitic tumor models (*37,38*).

Our biodistribution results confirm the nonspecific accumulation of nontargeted SCKs in solid tumors, but they also suggest FR-specific interaction of folated SCKs in small tumors. In fact, coadministration of excess folic acid led to competitive block of ^{64}Cu-TETA-SCK-folate uptake in KB xenografts at 4 h after injection (Fig. 3A), whereas it had no noticeable effect on ^{64}Cu-TETA-SCK uptake (Fig. 3B). Furthermore, SCK tumor uptake was seen to strongly depend on tumor weight: the smaller the tumor, the higher the specific SCK uptake. This is reasonably due to the presence of necrotic areas in big, fast-growing solid tumors, which hamper extravasation of blood-borne long-circulating molecules. This finding also explains the high variability in tumor uptake. In fact, tumor size varied considerably within each group and among different groups of mice used in the biodistribution study. However, effective uptake in small tumors is a key feature of potential systems for drug delivery, since it allows for the diagnosis and treatment of early-stage neoplasms.

SCK distribution in solid tumors was evaluated by means of dual-tracer autoradiography. In this series of experiments, we used mice bearing 2-wk-old subcutaneous KB tumor cell xenografts weighing 0.3–0.6 g. Mice were administered ^{64}Cu-labeled SCKs and ^{18}F-FDG separately, 24 and 1 h, respectively, before sacrifice. Digital autoradiography was then performed on 1-mm tumor slices shortly after sacrifice and 20 h later, to allow for complete ^{18}F decay. Within tumor tissues, both ^{64}Cu-labeled SCK-folate (Fig. 4A) and native SCK (Fig. 4B) exhibited a markedly heterogeneous distribution (which was confirmed in a second series of experiments, not reported here). In all tumor slices, sizeable zones appear that display no accumulation of either ^{18}F-FDG or nanoparticles and that reasonably correspond to necrotic areas. However, despite the general concordance of regional ^{18}F and ^{64}Cu accumulation within the tumor, some areas exhibit accumulation of only one radiotracer, either ^{18}F-FDG or ^{64}Cu-labeled SCK. This is due to the different mechanisms driving the accumulation of the administered radiotracers. In fact, ^{18}F-FDG is a small molecule that diffuses into tumor tissues and accumulates in areas of high metabolic activity (*39*), whereas macromolecules extravasate from hyperpermeable blood vessels and concentrate in vascularized tumor tissues regardless of tumor biochemistry.

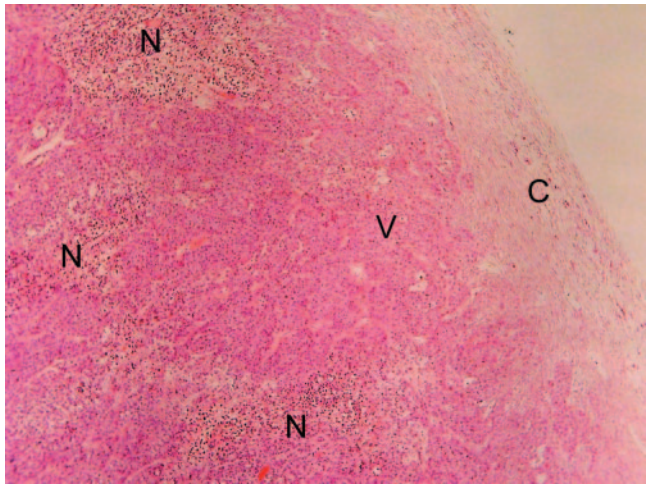

FIGURE 5. Cross-sectional slice from a tumor generated by subcutaneous inoculation of a *nu/nu* athymic mouse with 1×10^6 human KB cells. Tumor mass is enclosed in a capsule (C) and it is characterized by scattered necrotic regions (N) surrounded by viable tissues (V). (hematoxylin–eosin, ×40)

Histopathologically, these KB cell tumor xenografts revealed apoptotic foci with macrophage infiltration and scattered necrotic areas (Fig. 5), consistent with autoradiographic findings.

CONCLUSION

We have reported the synthesis and preliminary in vitro and in vivo evaluation of new folate-conjugated polymeric nanoparticles, suitable for both active and passive tumor targeting.

Previously reported procedures for the synthesis of SCKs were followed with minor modifications, and a global solution-state functionalization strategy has been successfully developed for attaching optimum numbers of targeting and imaging agents onto the SCK nanoparticles. Epifluorescence microscopy confirmed the specific interaction of FTSC-conjugated SCK-folate with FR-overexpressing tumor cells in vitro. After TETA conjugation, we developed a simple method to radiolabel SCK and SCK-folate with ^{64}Cu, which allowed us to perform in vivo biodistribution and autoradiography studies. Altogether, these studies confirmed that nanoparticle accumulation in solid tumors is achievable and that it is driven mainly by the EPR effect. In fact, both folated and nonfolated SCKs exhibited similar tumor uptake and distribution. However, FR-mediated uptake of SCKs in very small tumors was observed, suggesting the possible use of radiolabeled SCKs as drug delivery systems for imaging and treatment of early-stage tumors.

Downloaded from jnm.snmjournals.org by on March 15, 2017. For personal use only.

Although the focus of the current study has been on ^{64}Cu labeling and FR targeting, the same strategy also applies to other imaging or therapeutic agents and molecular targets. SCKs are versatile and multivalent platforms, as their surface can be easily functionalized with a panel of different ligands, chelating systems, prodrugs, genes, and so forth, for a more broad-spectrum targeting approach.

ACKNOWLEDGMENTS

The authors thank Nicole Fettig, Margaret Morris, Lynne Jones, and Terry Sharp for technical assistance in the biodistribution studies and Susan Adams for cell culture. This project has been funded in part by the National Cancer Institute (NCI), the National Institutes of Health (NIH) (N01-CO-27103), the U.S. Department of Energy (DE-FG02-87ER60512), and by a NIH Chemistry–Biology Interface Pathway Training Grant Fellowship. The production of ^{64}Cu at Washington University School of Medicine is supported by NCI grant R24 CA86307.

REFERENCES

1. Moghimi SM, Hunter AC, Murray JC. Long-circulating and target-specific nanoparticles: theory to practice. *Pharmacol Rev.* 2001;53:283–318.
2. Guccione S, Li KCP, Bednarski MD. Vascular-targeted nanoparticles for molecular imaging and therapy. *Methods Enzymol.* 2004;386:219–236.
3. Storm G, Belliot SO, Daemen T, Lasic DD. Surface modification of nanoparticles to oppose uptake by the mononuclear phagocyte system. *Adv Drug Deliv Rev.* 1995;17:31–48.
4. Brigger I, Dubernet C, Couvreur P. Nanoparticles in cancer therapy and diagnosis. *Adv Drug Deliv Rev.* 2002;54:631–651.
5. Brannon-Peppas L, Blanchette JO. Nanoparticle and targeted systems for cancer therapy. *Adv Drug Deliv Rev.* 2004;56:1649–1659.
6. Munn LL. Aberrant vascular architecture in tumors and its importance in drug-based therapies. *Drug Discov Today.* 2003;8:396–403.
7. Hobbs SK, Monsky WL, Yuan F, et al. Regulation of transport pathways in tumor vessels: role of tumor type and microenvironment. *Proc Natl Acad Sci USA.* 1998;95:4607–4612.
8. Padera TP, Kadambi A, di Tomaso E, et al. Lymphatic metastasis in the absence of functional intratumor lymphatics. *Science.* 2002;296:1883–1886.
9. Hood JD, Bednarski M, Frausto R, et al. Tumor regression by targeted gene delivery to the neovasculature. *Science.* 2002;296:2404–2407.
10. Winter PM, Caruthers SD, Kassner A, et al. Molecular imaging of angiogenesis in nascent Vx-2 rabbit tumors using a novel $\alpha_v\beta_3$-targeted nanoparticle and 1.5 tesla magnetic resonance imaging. *Cancer Res.* 2003;63:5838–5843.
11. Dubey PK, Mishra V, Jain S, Mahor S, Vyas SP. Liposomes modified with cyclic RGD peptide for tumor targeting. *J Drug Target.* 2004;12:257–264.
12. Li L, Wartchow CA, Danthi SN, et al. A novel antiangiogenesis therapy using an integrin antagonist or anti-Flk-1 antibody coated ^{90}Y-labeled nanoparticles. *Int J Radiat Oncol Biol Phys.* 2004;58:1215–1227.
13. Pan D, Turner JL, Wooley KL. Shell cross-linked nanoparticles designed to target angiogenic blood vessels via $\alpha_v\beta_3$ receptor-ligand interactions. *Macromolecules.* 2004;37:7109–7115.
14. Thomas TP, Patri AK, Myc A, et al. In vitro targeting of synthesized antibody-conjugated dendrimer nanoparticles. *Biomacromolecules.* 2004;5:2269–2274.
15. Farokhzad OC, Jon S, Khademhosseini A, Tran T-NT, LaVan DA, Langer R. Nanoparticle-aptamer bioconjugates: a new approach for targeting prostate cancer cells. *Cancer Res.* 2004;64:7668–7672.
16. Stella B, Arpicco S, Peracchia MT, et al. Design of folic acid-conjugated nanoparticles for drug targeting. *J Pharm Sci.* 2000;89:1452–1464.
17. Pan D, Turner JL, Wooley KL. Folic acid-conjugated nanostructured materials designed for cancer cell targeting. *Chem Commun (Camb).* 2003;7:2400–2401.
18. Pan XQ, Wang H, Lee RJ. Antitumor activity of folate receptor-targeted liposomal doxorubicin in a KB oral carcinoma murine xenograft model. *Pharm Res.* 2003;20:417–422.
19. Oyewumi MO, Yokel RA, Jay M, Coakley T, Mumper RJ. Comparison of cell uptake, biodistribution and tumor retention of folate-coated and PEG-coated gadolinium nanoparticles in tumor-bearing mice. *J Control Release.* 2004;95:613–626.
20. Choi H, Choi SR, Zhou R, Kung HF, Chen I-W. Iron oxide nanoparticles as magnetic resonance contrast agent for tumor imaging via folate receptor-targeted delivery. *Acad Radiol.* 2004;11:996–1004.
21. Hattori Y, Maitani Y. Enhanced in vitro DNA transfection efficiency by novel folate-linked nanoparticles in human prostate cancer and oral cancer. *J Control Release.* 2004;97:173–183.
22. Gabizon A, Shmeeda H, Horowitz AT, Zalipsky S. Tumor cell targeting of liposome-entrapped drugs with phospholipid-anchored folic acid-PEG conjugates. *Adv Drug Del Rev.* 2004;56:1177–1192.
23. Antony AC. Folate receptors. *Annu Rev Nutr.* 1996;16:501–521.
24. Garin-Chesa P, Campbell I, Saigo PE, Lewis JLJ, Old LJ, Rettig WJ. Trophoblast and ovarian cancer antigen LK26: sensitivity and specificity in immunopathology and molecular identification as a folate-binding protein. *Am J Pathol.* 1993;142:557–567.
25. Leamon CP, Reddy JA. Folate-targeted chemotherapy. *Adv Drug Del Rev.* 2004;56:1127–1141.
26. Ke C-Y, Mathias CJ, Green MA. The folate receptor as a molecular target for tumor-selective radionuclide delivery. *Nucl Med Biol.* 2003;30:811–817.
27. Wooley KL. Shell cross-linked polymer assemblies: nanoscale constructs inspired from biological systems. *J Polym Sci [A1].* 2000;38:1397–1407.
28. Becker ML, Remsen EE, Pan D, Wooley KL. Peptide-derivatized shell-cross-linked nanoparticles. 1. Synthesis and characterization. *Bioconjug Chem.* 2004;15:699–709.
29. Sun X, Anderson CJ. Production and applications of copper-64 radiopharmaceuticals. *Methods Enzymol.* 2004;386:237–261.
30. McCarthy DW, Shefer RE, Klinkowstein RE, et al. Efficient production of high specific activity ^{64}Cu using a biomedical cyclotron. *Nucl Med Biol.* 1997;24:35–43.
31. Mathias CJ, Wang S, Lee RJ, Waters DJ, Low PS, Green MA. Tumor-selective radiopharmaceutical targeting via receptor-mediated endocytosis of gallium-67-deferoxamine-folate. *J Nucl Med.* 1996;37:1003–1008.
32. Qi K, Ma Q, Remsen EE, Clark CGJ, Wooley KL. Determination of the bioavailability of biotin conjugated onto shell cross-linked (SCK) nanoparticles. *J Am Chem Soc.* 2004;126:6599–6607.
33. Lewis MR, Kao JY, Anderson AL, Shively JE, Raubitschek A. An improved method for conjugating monoclonal antibodies with N-hydroxysulfosuccinimidyl DOTA. *Bioconjug Chem.* 2001;12:320–324.
34. McHugh M, Cheng YC. Demonstration of a high affinity folate binder in human cell membranes and its characterization in cultured human KB cells. *J Biol Chem.* 1979;254:11312–11318.
35. Reddy JA, Abburi C, Hofland H, et al. Folate-targeted, cationic liposome-mediated gene transfer into disseminated peritoneal tumors. *Gene Ther.* 2002;9:1542–1550.
36. Pan XQ, Wang H, Lee RJ. Boron delivery to a murine lung carcinoma using folate receptor-targeted liposomes. *Anticancer Res.* 2002;22:1629–1634.
37. Leamon CP, Cooper SP, Hardee GE. Folate-liposome-mediated antisense oligodeoxynucleotide targeting to cancer cells: evaluation in vitro and in vivo. *Bioconjug Chem.* 2003;14:738–747.
38. Gabizon A, Horowitz AT, Goren D, Tzemach D, Shmeeda H, Zalipsky S. In vivo fate of folate-targeted polyethylene-glycol liposomes in tumor-bearing mice. *Clin Cancer Res.* 2003;9:6551–6559.
39. Pauwels EKJ, Ribeiro MJ, Stoot JHMB, McCready VR, Bourguignon M, Maziere B. FDG accumulation and tumor biology. *Nucl Med Biol.* 1998;25:317–322.

Downloaded from jnm.snmjournals.org by on March 15, 2017. For personal use only.

The Journal of NUCLEAR MEDICINE

^{64}Cu-Labeled Folate-Conjugated Shell Cross-Linked Nanoparticles for Tumor Imaging and Radiotherapy: Synthesis, Radiolabeling, and Biologic Evaluation

Raffaella Rossin, Dipanjan Pan, Kai Qi, Jeffrey L. Turner, Xiankai Sun, Karen L. Wooley and Michael J. Welch

J Nucl Med. 2005;46:1210-1218.

This article and updated information are available at:
http://jnm.snmjournals.org/content/46/7/1210

Information about reproducing figures, tables, or other portions of this article can be found online at:
http://jnm.snmjournals.org/site/misc/permission.xhtml

Information about subscriptions to JNM can be found at:
http://jnm.snmjournals.org/site/subscriptions/online.xhtml

The Journal of Nuclear Medicine is published monthly.
SNMMI | Society of Nuclear Medicine and Molecular Imaging
1850 Samuel Morse Drive, Reston, VA 20190.
(Print ISSN: 0161-5505, Online ISSN: 2159-662X)

© Copyright 2005 SNMMI; all rights reserved.

SNMMI SOCIETY OF NUCLEAR MEDICINE AND MOLECULAR IMAGING